

FLUX RELAXATION AFTER TWO OUTBURSTS OF THE MAGNETAR SGR 1627–41 AND POSSIBLE HARD X-RAY EMISSION

HONGJUN AN^{1,*}, ANDREW CUMMING², AND VICTORIA M. KASPI²

¹DEPARTMENT OF ASTRONOMY AND SPACE SCIENCE, CHUNGBUK NATIONAL UNIVERSITY, CHEONGJU, 28644, REPUBLIC OF KOREA

²DEPARTMENT OF PHYSICS & MCGILL SPACE INSTITUTE, RUTHERFORD PHYSICS BUILDING, MCGILL UNIVERSITY, 3600 UNIVERSITY STREET, MONTREAL, QUEBEC, H3A 2T8, CANADA

Draft version September 2, 2018

ABSTRACT

We report on the long-term flux relaxation of the magnetar SGR 1627–41 after its 2008 outburst, and evidence for hard X-ray excess measured with *NuSTAR*. We use new observations made with *Chandra* and *XMM-Newton*, and an archival *NuSTAR* observation which add flux measurements at ~ 2000 days into quiescence after the 2008 outburst. We find that the source flux has further declined since the last measurement made in 2011, ~ 1000 days after the outburst in 2008. This trend is similar to the relaxation after the source’s 1998 outburst. We use crustal cooling models to reproduce the flux relaxation; if the whole surface of the star is heated in the outbursts, the modeling suggests that the 2008 outburst of SGR 1627–41 deposited energy into the inner crust and that the core temperature of SGR 1627–41 is low ($T_c \lesssim 10^8$ K) as previously suggested. On the other hand, if only a small fraction of the surface is heated or the temperature in the crust reached the melting temperature, relaxation at early times requires another emission mechanism. Finally, we report on evidence for hard X-ray emission in SGR 1627–41 which follows the observational correlation suggested by Kaspi & Boydston (2010) in magnetars.

Keywords: pulsars: individual (SGR 1627–41) — stars: magnetars — stars: neutron — X-rays: bursts

1. INTRODUCTION

Magnetars are neutron stars which have very strong magnetic fields (Thompson & Duncan 1995, 1996), typically $B > 10^{14}$ G, as inferred from their spin properties, with some exceptions (SGR 0418+5729, Swift J1822.3–1606; Rea et al. 2010; Scholz et al. 2014). Their emission is almost all in the X-ray band and is believed to be produced by decay of the enormous internal magnetic fields. Hence, magnetars often have larger X-ray luminosity than their rotational power. They exhibit diverse observational properties (Olausen & Kaspi 2014; Mereghetti et al. 2015; Kaspi & Beloborodov 2017) such as short soft gamma-ray bursts, more dramatic long X-ray outbursts and giant flares, and spectral turn-over in the hard X-ray band (~ 10 keV). See also the online magnetar catalog for various observational properties of magnetars.¹

Emission from magnetars is believed to be supported by the strong magnetic field; internal decay of the magnetic field produces heat which is released at the surface as thermal emission (Thompson et al. 2002). The thermal spectrum is further modified in the atmosphere due to absorption or in the magnetosphere due to resonant scattering (Fernández & Thompson 2007), and a non-thermal tail is seen at higher energies. Intriguingly, rising trends in their spectral energy distributions (SEDs) above 10 keV were seen in some magnetars (Kuiper et al. 2006). The possible origin of this emission was discussed by several authors (Heyl & Hernquist 2005; Thompson & Beloborodov 2005; Baring & Harding 2007; Beloborodov & Thompson 2007; Wadiasingh et al.

2018), and recently magnetar hard X-ray emission was investigated with a coronal outflow model (Beloborodov 2013) for some magnetars (e.g., 1E 1841–045, 4U 0142+61, 1E 2259+586; An et al. 2013; Vogel et al. 2014; Tendulkar et al. 2015), and was used for inferring the emission geometry. Observationally, for hard X-ray bright magnetars, Kaspi & Boydston (2010) found a correlation between the degree of spectral break and the spin-inferred magnetic field strength, which can give further insights into the hard X-ray emission mechanism (e.g., Enoto et al. 2017).

The mechanism by which the magnetic energy is released in magnetars is still uncertain (Beloborodov & Li 2016). As the strong magnetic fields inside a magnetar evolve, the external field can be twisted and the crust distorted, depositing energy both inside and outside the star (Thompson et al. 2002). Energy deposited in shallow regions of the crust may explain the observed surface luminosities of persistent magnetars (Kaminker et al. 2006; Beloborodov & Li 2016), and may be responsible for the transient emission seen in magnetar outbursts, in which the X-ray luminosity of the star increases by orders of magnitude. These outbursts have been modeled as due to release of stress in the crust by temperature-dependent plastic motions (Levin & Lyutikov 2012; Beloborodov & Levin 2014; Thompson et al. 2017). Magnetospheric activity can also lead to energy being deposited in the outer layers of the star (Li & Beloborodov 2015).

The transient relaxation of a magnetar after the outburst can give clues as to the nature and location of the heating that causes the outburst, as well as the response of the star and the magnetosphere. The flux relaxation after outburst has been modeled by both crust

*hjan@chungbuk.ac.kr

¹ <http://www.physics.mcgill.ca/pulsar/magnetar/main.html>

Table 1
Summary of observations used in this work

Observatory	ObsId	Start time (MJD)	Instruments	observation mode	Exposure (ks)	Comment
<i>Chandra</i>	15625	56374	ACIS-I	Imaging	10	10' off-axis
<i>XMM-Newton</i>	0742650101	57071	MOS1,MOS2,PN	Full window	40	medium filters
<i>NuSTAR</i>	30160002002	57181	FPMA, FPMB	...	100	...

cooling and untwisting of the external magnetosphere. In the crust cooling models (e.g., Lyubarsky et al. 2002; Kouveliotou et al. 2003; Pons & Rea 2012; Scholz et al. 2014), energy is deposited inside the star, and the subsequent cooling is calculated assuming crust properties and the energy deposition profile. In untwisting models (e.g., Beloborodov 2009), the outburst suddenly twists the external magnetic field in a specified way, and then the flux relaxes to the quiescent level as the twist unwinds. Both mechanisms could contribute to the transient relaxation, but with different trends over time.

SGR 1627–41 (hereafter SGR1627) was discovered during an outburst in 1998 (Woods et al. 1999) and exhibited another outburst in 2008 (Esposito et al. 2008). The spin-down rate ($P = 2.59$ s) and its first derivative ($\dot{P} = 1.9 \times 10^{-11}$) were measured after the 2008 outburst when the source was bright (Esposito et al. 2009). This implies that the surface dipolar magnetic field strength is $B = 2 \times 10^{14}$ G, well within the range for magnetars. The flux relaxations after the outbursts have been relatively well measured (Kouveliotou et al. 2003; Esposito et al. 2008; An et al. 2012).

The fact that two outbursts have been observed from the same source is interesting for the crust cooling model because it could remove some of the degeneracy between the parameters of the model; the shape of the cooling curve depends on both crust properties and the energy deposited, but the crust properties should be the same from outburst to the next. In addition, the long timescales of thousands of days over which the flux decay has been observed make the light curves possibly sensitive to the interesting physics of the crust/core boundary. For example, it has been suggested that the pasta phase expected at these densities may give a low conductivity (Pons et al. 2013; Horowitz et al. 2015). Because the published observations of the decay following the most recent 2008 outburst extend to ~ 1000 days, with the possibility that the source could further drop in flux, the interpretation in the context of the crust cooling model is uncertain. With different assumptions about the heating profile, An et al. (2012) concluded that the neutron star core temperature could be higher than previously thought, whereas Deibel et al. (2017) assumed a lower core temperature and made predictions for the future flux evolution that depended on the parameters chosen for the inner crust.

We report on new observations of SGR1627 made with *Chandra* and *XMM-Newton* and an archival *NuSTAR* observation. These observations sample very late-time transient relaxation of the source, $\gtrsim 2000$ days into quiescence, for which modeling the relaxation trend provides a new test of the crust cooling and the magnetospheric untwisting models, and may give us new insights into the energy deposition in outbursts of magnetars. In section 2, we describe the observational data and present

our analysis results. We show our modeling results in section 3 and then discuss and conclude in section 4.

2. DATA ANALYSIS AND RESULTS

We used a 10-ks *Chandra* and a 40-ks *XMM-Newton* observation made on MJDs 56374 and 57071, respectively (Table 1). The *Chandra* data are reprocessed with `chandra_repro` of CIAO 4.8 along with CALDB 4.7.2 to use the most recent calibration files, and the 40-ks *XMM-Newton* data are processed with `eproc` and `emproc` of SAS 20160201_1833-15.0.0. Note that in the *Chandra* observation SGR1627 was observed with a $\gtrsim 10'$ offset from the optical axis, hence the effective photon-collecting area was small, and only a few events were detected near the source position. We also analyzed archival 100-ks *NuSTAR* data (Fornasini et al. 2017), taken ~ 100 days after the *XMM-Newton* observation (Figure 1). The data were processed with `nupipeline` integrated in the HEASOFT 6.19 along with the HEASARC remote CALDB. We further process the data for analyses below. We also use published results (Kouveliotou et al. 2003; Esposito et al. 2008; An et al. 2012) for constructing and modeling SGR1627’s flux relaxation trends.

2.1. *XMM-Newton* Data Analysis

We measure the spectrum of SGR1627 with the *XMM-Newton* data because these provide by far the best statistics. Although SGR1627 was in its late stage of transient cooling and thus is very faint, it is visible in each of MOS and PN exposures. We extracted source events within a $R = 16''$ circle around the source position, collecting 310 events (PN and MOS1,2 combined in the 0.5–10 keV band) in this region. Background events were extracted in a source-free $R = 32''$ circular region, 200'' north of SGR1627 (580 events); the detection significance is $\sim 8\sigma$. We calculated spectral response files using the `rmfgen` and the `arfgen` tools of SAS. We group the spectra to have at least 5 counts per energy bin and use an absorbed power-law or an absorbed blackbody model. Unless otherwise stated, we use `wilm` abundance (Wilms et al. 2000) and `verner` cross section (Verner et al. 1996) because these are used for cross calibration of the *NuSTAR* data with other X-ray satellites (Madsen et al. 2015).

We fit the spectra using l -statistic in XSPEC 12.9.0n (Loredo 1992). The best-fit N_{H} and Γ are consistent with the previous results (e.g., Esposito et al. 2008). We, however, find that the source flux declined by a factor of 2–3 compared with the last measurement of $F_{2-10 \text{ keV}} = 2.7 \pm 0.4 \times 10^{-13} \text{ erg cm}^{-2} \text{ s}^{-1}$ made in 2011. The significance of the flux drop is $\sim 3\sigma$ if we fit N_{H} as well, and larger if we hold N_{H} fixed at the value measured by Esposito et al. (2008). The blackbody model can also explain the data, with high surface temperature compared with other magnetars in quiescence. Because the power-law model is slightly better

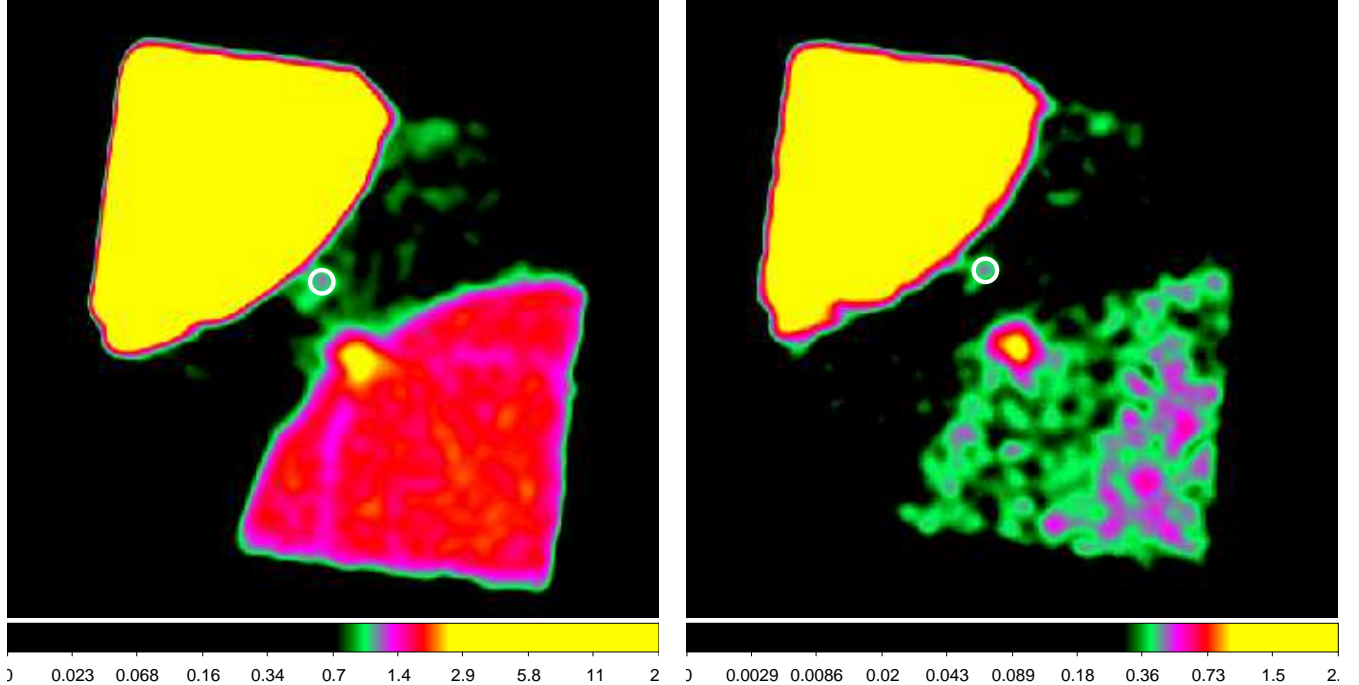


Figure 1. Soft- and hard-band images of the *NuSTAR* observation in the 3–10 keV (left) and 10–20 keV bands (right). The magnetar SGR1627 is shown in a circle. The image is smoothed and the color scale is changed for better legibility. The bright point source $\sim 2'$ south-west of SGR1627 is CXOU J163547.0–473739 (Fornasini et al. 2017), and the large bright patterns in the north east and south west are produced by stray light (photons that are not reflected by the focusing mirrors) or ghost rays (photons that are reflected only once) from the nearby (but outside the FoV) bright sources GX 340+0 and 4U 1624–49 (Fornasini et al. 2017). See Madsen et al. (2017) for more details about stray light and ghost rays.

and the previous measurements were all done with that model, we use the power-law flux for the light curve below. The results of the fitting are summarized in Table 2. We also used a different absorption model, `anqr` abundance and the `bcmc` cross section (Anders & Grevesse 1989; Balucinska-Church & McCammon 1992) for comparison with the 2011 measurements, and find that the best-fit parameters do not change significantly. In this fit, the best-fit N_{H} is smaller and the 2–10 keV flux is $\sim 10\%$ larger.

2.2. *Chandra* Data Analysis

As we noted above, there are only a few events detected near the source position in the *Chandra* data, and hence we measure a flux upper limit only. For this, we used a circular aperture with $R = 5''$ for the source and an annular aperture with $R_{\text{in}} = 10''$ and $R_{\text{out}} = 20''$ for the background. In these apertures, we find 1 event in the source region and 16 events in the background region in the 2–10 keV band. Since it is impractical to perform a spectral fit with these small numbers of events, we measure a flux upper limit.

We first calculated the effective area for the source region using the `specextract` tool of CIAO and used the *XMM-Newton*-measured power-law spectral shape as our source model because a power-law model fits the *XMM-Newton* data better than a blackbody model does, and the previous results are made with a power-law model. We then adjust the normalization of the source model (i.e., flux) and fold it with the effective area until the chance probability (Poisson statistic) of having 1 or less event within a $R = 5''$ circle in the 2–10 keV band is

smaller than 10%, considering the background as well. We find this flux value to be $1.7 \times 10^{-13} \text{ erg s}^{-1} \text{ cm}^{-2}$ and set this as the 90% upper limit for the source flux at the observation epoch. Note that this is also smaller than the 2011 measurement. Our measurements of the source fluxes are shown in Figure 2.

2.3. *NuSTAR* Data Analysis

In the *NuSTAR* observation, SGR1627 was very faint, dominated by background. The magnetar was detected only at the $\lesssim 6\sigma$ level in the 3–25 keV band, and so the data are insufficient for determining the spectrum accurately. However, it can provide a consistency check for the *XMM-Newton* results, and thus we perform a spectral analysis in the 3–10 keV band. We extracted spectra using $R = 20''$ apertures for two *NuSTAR* modules FPMA and FPMB, and generated response files using the `nuproducts` tool. We then bin the spectra to have at least 5 events per spectral bin and fit the spectra in *XSPEC* with an absorbed power-law model using the l statistic.

The power-law index we measure is somewhat smaller (but not significantly) than that reported by Fornasini et al. (2017), but agrees with the *XMM-Newton* result. The measured spectral index and the 2–10-keV-extrapolated flux are 3.4 ± 1.0 and $12 \times 10^{-14} \text{ erg cm}^{-2} \text{ s}^{-1}$ (Table 2). We did not attempt to fit the *NuSTAR* data with a blackbody model because of the lack of sensitivity of *NuSTAR* below 3 keV. Because the background dominates the spectra in this analysis, the results may be sensitive to the background selection. We therefore tried with backgrounds taken from different

Table 2
Fit results for the *XMM-Newton* and the *NuSTAR* data

Model ^a	Inst.	Energy (keV)	N_{H} (10^{22}cm^{-2})	Γ/kT (\dots/keV)	Γ_2	E_B (keV)	Flux	$lstat/dof$
PL	X	0.3–10	13 ± 5	2.6 ± 0.8	10^{+4}_{-3}	41.6/54
PL	X	0.3–10	10^c	2.0 ± 0.3	8 ± 1	42.4/55
BB	X	0.3–10	7 ± 3	1.3 ± 0.2	6 ± 1	43.5/54
BB	X	0.3–10	10^c	1.1 ± 0.1	7 ± 1	44.6/55
PL	N	3–20	10^c	1.0 ± 0.6	4^{+2}_{-1}	53.2/55
PL	N	3–10	10^c	3.4 ± 1.0	6^{+3}_{-2}	33.1/39
PL	X+N	0.3–20	10^c	1.8 ± 0.3	6^{+2}_{-1}	97.7/112
BPL	X+N	0.3–20	10^c	2.2 ± 0.3	-0.4 ± 1.2	8.9 ± 2.6	4^{+2}_{-1}	88.8/110

^aPL: power law, BB: Blackbody.

^bAbsorption corrected flux in units of $10^{-14}\text{erg cm}^{-2}\text{s}^{-1}$ in the 2–10 keV band for *XMM-Newton* and in the 3–10 keV band for *NuSTAR* or *XMM-Newton + NuSTAR*.

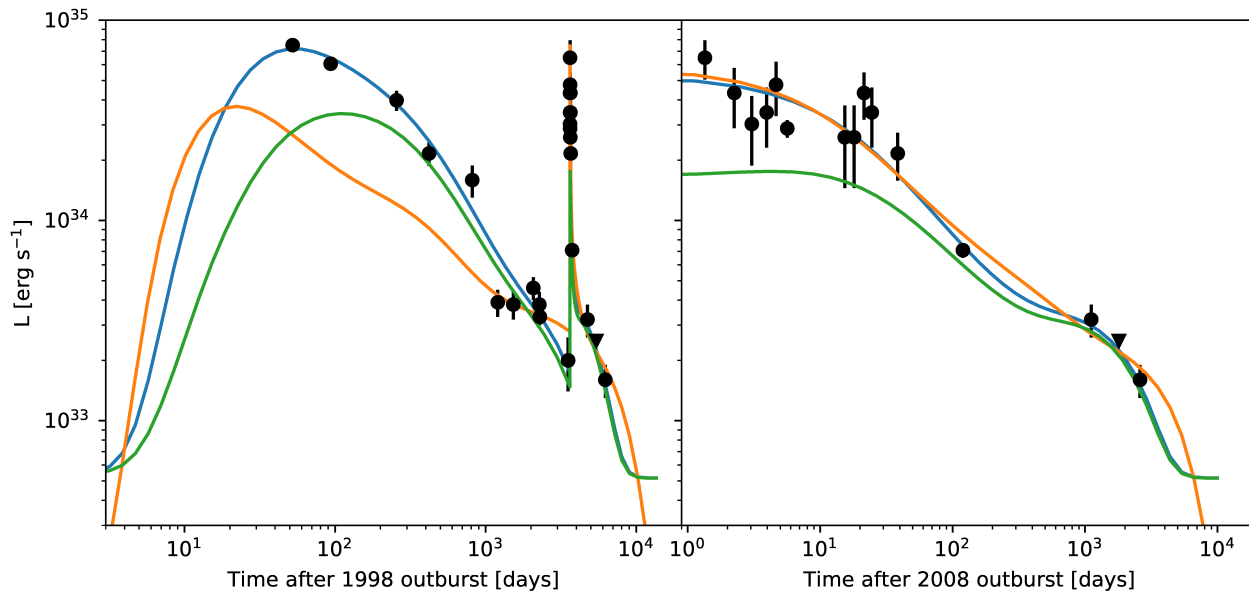


Figure 2. Flux relaxation data after the 1998 (left) and the 2008 (right) outbursts and crust cooling models (solid lines) for SGR1627. *Blue*: heating of the whole surface as in Deibel et al. (2017). To match the 2008 outburst at late times, we include heating in the inner crust. *Orange*: only 10% of the neutron star surface is heated, resulting in larger crust temperatures. The early part of the light curve reaches a maximum luminosity set by neutrino emission (Pons & Rea 2012). By reducing the neutron star surface gravity, we are able to fit the late time cooling without any inner crust heating in the 2008 outburst in this case. *Green*: Same as blue, but with the crust temperature limited to be less than the melting temperature. The luminosities are calculated with 2–10 keV fluxes assuming a distance of 11 kpc (Corbel et al. 1999). The details of the heating profile for each model are given in the caption of Figure 4.

regions and found that the results do not change significantly. We report the best-fit parameters in Table 2. Note that the uncertainty for the flux measurement is large, so we check to see if it is consistent with zero by scanning the photon index and flux with the `steppar` command of `XSPEC`. We find that the flux is not consistent with zero at the 99% confidence level.

2.4. Broadband X-ray Spectral Analysis

In the *NuSTAR* data analysis, we find evidence for spectral hardening with energy, as has been seen in some magnetars (Kuiper et al. 2006; Vogel et al. 2014; An et al. 2015; Tendulkar et al. 2015). The spectral index for a simple power-law model is 1 ± 0.6 when fitting the data in the 3–20 keV band, much smaller than 3.4 ± 1.0 measured in the soft 3–10 keV band (Table 2). This trend can be seen in the spectrum (Figure 3). We note that the source is clearly detected up to ~ 20 keV (see also Fornasini et al. 2017), and is brighter compared

to the background at higher energies than at lower energies. In order to investigate this further, we fit the *NuSTAR* and the *XMM-Newton* data jointly. Although the observations are separated by ~ 100 days, no large outburst has been seen during this time and the soft-band source spectrum seems not to have changed; the 3–10 keV *NuSTAR* spectra are consistent with the *XMM-Newton* one; so jointly fitting the spectra is unlikely to suffer from systematic errors due to different flux levels.

We fit the 0.5–10 keV *XMM-Newton* and the 3–20 keV *NuSTAR* data jointly with an absorbed power-law or an absorbed broken power-law model, holding N_{H} fixed at 10^{23}cm^{-2} . Due to the paucity of counts, both models explain the data reasonably when using the χ^2 statistic with `gehrels` weighting (Gehrels 1986); χ^2/dof 's are 45.17/112 and 41.55/110 for the power-law and the broken power-law models, respectively, and the f -test probability that the additional parameters are unnecessary is 0.01. Because we are concerned with the results be-

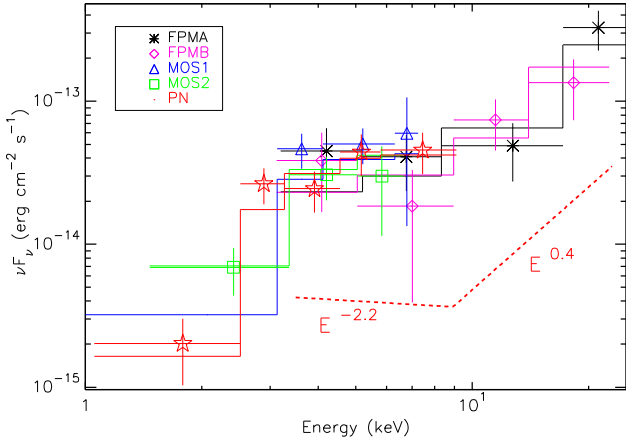


Figure 3. Broadband X-ray spectral energy distribution (SED, $E^2 \frac{dN}{dE}$) measured with *XMM-Newton* and *NuSTAR* (points with error bars) and the best-fit broken power-law model (solid lines). The spectra measured with *XMM-Newton* are shown in blue (MOS1), green (MOS2) and red (PN). *NuSTAR* spectra are shown in black (FPMA) and magenta (FPMB). We also show a broken power-law line (red dashed) separately for clarity.

ing sensitive to the statistics employed, we further test the fits with the l statistic (5 cts per bin) or c statistic (1 cts per bin; Cash 1979). For these, we find that the best-fit spectral parameters are consistent with those obtained with the χ^2 fit (Table 2), and the Akaike information criterion (Akaike 1974) also tells us that the broken power-law model is favored over the simple power-law model.

2.5. Timing Analysis

We perform a timing analysis to search for pulsations with the *XMM-Newton*/PN and the *NuSTAR* data which were both taken with sufficient timing resolution (72 ms for *XMM-Newton*/PN and ~ 2 ms for *NuSTAR*). The pulse period and the first derivative of SGR1627 were measured to be $P = 2.59439$ s and $\dot{P} = 1.9 \times 10^{-11}$ on MJD 51259 (Esposito et al. 2009). When extrapolated to the epochs of the observations we are using, the expected period is $P \simeq 2.60$ s. We therefore searched for pulsations between $P = 2.5$ s and $P = 2.7$ s using the H test (de Jager et al. 1989), but found no significant pulsation in the data. This is not surprising given the fact that the pulsations were detected only when the source was bright after the 2008 outburst; the pulsed fraction is low (0.13; Esposito et al. 2009) and so the signal-to-noise ratio is not likely high enough for a detection when the source is faint.

3. MODELING THE FLUX RELAXATION OF SGR1627

We compile data taken for two outbursts of SGR1627 to study the source’s transient relaxation. We added the measurements we made in this work to the data reported by Kouveliotou et al. (2003), Esposito et al. (2008) and An et al. (2012). The new observations sample the 2008 cooling trend at ~ 1800 days and ~ 2500 days, and ~ 2600 days, (Figure 2) providing constraints on the late time cooling, which depends on the properties of the inner crust and magnetosphere of SGR1627, and energy deposition profiles of the outbursts, and/or the magnetospheric twist/untwist. We first summarize previous work

on crust cooling applied to SGR1627 and then present new models that fit the latest flux measurements.

3.1. Previous work

Kouveliotou et al. (2003) were able to reproduce the flux decay of SGR1627 following its outburst in 1998 using a crust cooling model in which they deposited $\sim 10^{44}$ ergs in the crust. The temperature profile they assumed right after the outburst was guided by the variation of specific heat capacity with depth (in the outer crust, the specific heat is dominated by the nuclear lattice, whereas it is strongly suppressed in the inner crust when the neutrons become superfluid). They chose a low core temperature $\ll 10^8$ K to reproduce the drop in luminosity seen at late times (see their Fig. 1).

After the second outburst in 2008, An et al. (2012) compared the 2–10 keV luminosity decays of both outbursts with crust cooling models. They considered models in which energy is deposited instantaneously in the outer crust down to a density ρ_{\max} , and then the crust is allowed to thermally relax. They assumed spherical symmetry so that the heating is over the whole stellar surface, and neutron star parameters $M = 1.3 M_{\odot}$, $R = 12$ km, $B = 2 \times 10^{14}$ G, $Q_{\text{imp}} = 3$, where M and R are the neutron star mass and radius, B is the polar magnetic field, and Q_{imp} is the impurity parameter that determines the conductivity of the inner crust (Itoh & Kohyama 1993). Modeling the 1998 and 2008 outbursts, they found that the amount of energy deposited must be about ten times greater (energy density $E_{25} = E/10^{25}$ erg cm $^{-3} \sim 1$ for 2008 and $E_{25} \sim 10$ for 1998), and deeper (up to a density $\rho_{\max} \approx 3 \times 10^{10}$ g cm $^{-3}$ for 2008 and $\rho_{\max} \approx 2 \times 10^{11}$ g cm $^{-3}$ for 1998) for the 1998 outburst compared to the 2008 outburst, to match its brighter and longer outburst. With these choices the shape of the outbursts could be reproduced for times $\lesssim 1000$ days.

An et al. (2012) noted that the difference in outburst decay times has implications for the long timescale behavior. The luminosity at times ≈ 1000 days was similar for both outbursts. But the 2008 outburst decay was rapid enough and the heating shallow enough that the crust should have come back into thermal equilibrium with the core at ~ 1000 days. This implies a hot core with core temperature $T_c \approx 2 \times 10^8$ K (An et al. 2012). However, the 1998 outburst showed a further drop in luminosity by a factor of two that was observed in an observation taken several years after the outburst. This measurement is unexpected for a hot core, which should keep the crust temperature high, but the observed luminosity is within about $2\text{-}\sigma$ of the previous value.

Deibel et al. (2017) investigated whether different choices for the (poorly constrained) physics of the inner crust could explain the drop in luminosity in the last measurement after the 1998 outburst. In particular, they looked at the effect of a low thermal conductivity in the part of the inner crust that is thought to consist of a nuclear pasta phase. A low electrical conductivity for the pasta phase had been suggested by Pons et al. (2013) in the context of neutron star magnetic field evolution, and the effect of a corresponding low thermal conductivity in accreting neutron stars on thermal relaxation after accretion outbursts had been calculated by Horowitz et al. (2015). However, Deibel et al. (2017) showed that the

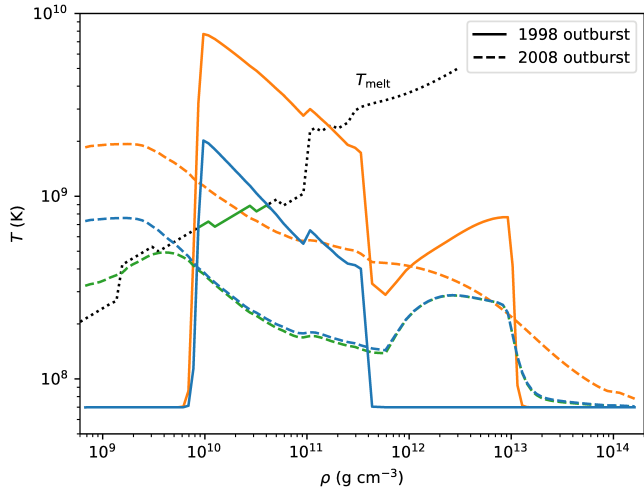


Figure 4. Temperature profiles at the end of each outburst (1998 solid curves, 2008 dashed curves) for the three models shown in Figure 2. The blue curves have $M = 1.4 M_{\odot}$, $R = 12$ km, and energy deposited over the entire stellar surface with $E_{25} = E/10^{25}$ erg $\text{cm}^{-3} = 13(0.9)$ in the outer (inner) crust for the 1998 outburst and $E_{25} = 0.9(10)$ in the outer (inner) crust for the 2008 outburst (total energies 6.1×10^{43} and 4.1×10^{43} ergs, respectively). The green curves correspond to the same model as the blue curves, but with the temperature limited to be less than the melting temperature (shown as the dotted curve in the Figure). The orange curves have $M = 1.2 M_{\odot}$, $R = 12.5$ km, and energy deposited over 10% of the neutron star surface at the magnetic pole, with $E_{25} = 130(130)$ in the outer (inner) crust for the 1998 outburst and $E_{25} = 4.0(0.0)$ in the outer (inner) crust for the 2008 outburst (total energies 1.6×10^{44} and 3.6×10^{42} ergs, respectively). The rapid increase in T_{melt} just above 10^{11} g cm^{-3} corresponds to the transition from $Z = 28$ to $Z = 44$ in the equilibrium crust model.

pasta layer does not delay cooling for the rapid heating thought to occur in a magnetar outburst (as opposed to the heating by accretion that occurs on timescales of years).

Instead, Deibel et al. (2017) found that the observations of An et al. (2012) could be made consistent with a colder core if the inner crust was also heated in the 2008 outburst. The amount of heating needed in the inner crust is comparable to that in the 1998 outburst (since both outbursts reach similar luminosities at times ~ 1000 days). This means that the energetics of the two outbursts are in fact similar, dominated by heat released in the inner crust, but they have very different decay times because of the different energies deposited in the outer crust. This picture is therefore quite different from the case with outer crust heating only as in An et al. (2012), where the two outbursts have different energies by an order of magnitude.

3.2. Models of the light curve

Now that we have two new observations showing that the flux has decreased further, we return to crust cooling models to see whether we can reproduce the observed flux decays and constrain the required heating and crust parameters². We model the two outbursts in the same calculation, i.e. we take into account the fact that the inner crust had not completely relaxed after the 1998 outburst when the 2008 outburst occurred. The basic parameters are similar to those in An et al. (2012): $M = 1.4 M_{\odot}$,

$R = 12$ km, $B = 2 \times 10^{14}$ G, $Q_{\text{imp}} = 1$, and core temperature $T_c = 7 \times 10^7$ K. It is important to note that when comparing to data, we compare only to the 2 – 10 keV luminosity and ignore the bolometric correction. Therefore our conclusions about energetics and whether we can match the observed luminosities should be taken as lower limits. We also do not consider or model the observed X-ray spectrum; we instead focus on the luminosity and see whether crust cooling models are able to reproduce the shape of the observed decay.

We briefly discuss the physics input of our model. The numerical grid extends from a density $\rho \approx 6 \times 10^8$ g cm^{-3} to the crust core boundary at $\rho \approx 1.4 \times 10^{14}$ g cm^{-3} (baryon density $n_b = 0.08$ fm $^{-3}$). General relativistic corrections are included as an overall redshift of the time or luminosity. The composition of the crust is taken from the cold-catalyzed matter calculations of Haensel & Pichon (1994) and Douchin & Haensel (2001). We take the melting point to be when $\Gamma = Z^2 e^2 / ak_B T = 175$ (Potekhin & Chabrier 2000), where Z is the nuclear charge and a the inter-ion spacing. We do not include the effects of the magnetic field on the electron equation of state (this is important only for $\rho < 2 \times 10^8$ g $\text{cm}^{-3} B_{15}^{3/2} (0.5/Y_e)$, which lies off our grid). The heat capacity has contributions from electrons, the ion lattice, and neutrons, with the neutron superfluid gap taken from Schwenk et al. (2003). Neutrino emission from plasmon decay and pair annihilation (Schinder et al. 1987), neutrino bremsstrahlung (Haensel et al. 1996; Kaminker et al. 1999), and neutrino synchrotron (Bezchastnov et al. 1997) is included. We calculate the thermal conductivity tensor, including the effect of the quantizing magnetic field, using the results for electron-phonon, electron-impurity, and electron-ion scattering summarized in Potekhin et al. (2015).³ For computational convenience, we use the envelope model results from Potekhin & Yakovlev (2001) to calculate the flux at the outer boundary (although as discussed by Scholz et al. (2014) this can lead to a tens of percent underestimate of the flux because the outer layers of the grid are not necessarily isothermal at high temperatures). In models which heat the entire surface of the neutron star, we solve an angle-averaged heat equation, averaged over latitude assuming a dipole magnetic field, following Greenstein & Hartke (1983). We have checked that this matches adequately with the more computationally intensive approach of following each local patch on the star separately and then summing the light curves.

We first assume spherical symmetry, i.e. heating across the entire neutron star surface, as assumed by An et al. (2012) and Deibel et al. (2017). The blue curve in Figure 2 shows a model similar to Deibel et al. (2017). It has an order of magnitude difference in heating in the outer crust ($\rho < 4 \times 10^{11}$ g cm^{-3}) between the two outbursts: $E_{25} = E/10^{25}$ erg $\text{cm}^{-3} = 13$ for 1998 and $E_{25} = 0.9$ for 2008. To match the observed luminosity at times $\gtrsim 1000$ days, we include a heating $E_{25} = 10$ in the inner crust for the 2008 outburst. No inner crust heating is included for the 1998 outburst, but it changes the 1998 light curve only slightly. After the inner crust begins to

² The code used to calculate the crust thermal relaxation is available at <https://github.com/andrewcumming/crustcool>.

³ Using the Fortran routine `condeg13.f` from the website of A. Potekhin, <http://www.ioffe.ru/astro/conduct/>

cool, the luminosity drops to a level set by the core temperature, here taken to be $T_c = 7 \times 10^7$ K. We show the temperature profiles in the crust after the outbursts in Figure 4.

Although it is possible that the heating occurs over most of the surface of the star (Thompson et al. 2017), the heated region could be substantially smaller. The orange curve in Figure 2 shows a model in which we heat only 10% of the neutron star surface (the magnetic field is assumed to be radial, so that the heated region is near the magnetic polar cap). Because the heated area is ten times smaller, the local energy density deposited in the crust is approximately an order of magnitude larger than in the previous model, making the crust significantly hotter. This has two effects. First, in the outer crust neutrino emission becomes important and limits the temperature. This gives a maximum luminosity that can be achieved at times of tens to hundreds of days, as discussed by Pons & Rea (2012). As can be seen in Figure 2, for this reason we are not able to match the observed light curve at these early times. The second effect of the high crust temperature is to increase the cooling time. However, this is offset by the enhanced conductivity associated with the radial field lines near the polar cap. We find that we can then match the decreasing luminosity at ≈ 3000 days by decreasing the neutron star gravity (the model shown has $M = 1.2 M_\odot$ and $R = 12.5$ km). Inner crust heating is not needed for the 2008 outburst; however it is needed in the 1998 outburst.

Another possible limitation at high temperature is that the crust melts. Whether this acts to limit the temperature depends on the mechanism of energy release. If the outburst results from dissipation due to a thermoplastic wave, as discussed by Beloborodov & Levin (2014) for example, the maximum temperature expected at a given depth is the local melting temperature T_{melt} . The green curve in Figure 2 shows a model with parameters the same as the blue curve, but we limit the temperature to be $T \leq T_{\text{melt}}$. Again, we find that we cannot match the luminosity observed at early times in each outburst.

To summarize, if a large fraction of the surface is heated, we find that we can match the light curves if the inner crust is heated in the 2008 outburst (and possibly in both outbursts). The energetics of each outburst are then similar, with the difference in outburst energy and timescale caused by a difference in the fraction of energy deposited in the outer crust. If instead only a small part of the neutron star surface is heated, or if the temperature in the crust is limited by the melting temperature, the initial parts of the outburst are too luminous to be reproduced by crust cooling models. In that case, another explanation is needed for the early time emission. It could be, for example, magnetospheric in origin, with the neutron star cooling taking over at late times.

Although we do not use a detailed model for magnetospheric relaxation in this work, a plausible relaxation scenario for the early time trend after the outbursts is the untwisting model (Beloborodov 2009; Li et al. 2016), which was used for explaining the transient relaxation of the magnetar XTE J1810–197 (Gotthelf & Halpern 2007; Alford & Halpern 2016). In this model, the external magnetic field is twisted due to sudden crustal motion, and then untwists with time. Ohmic dissipation

in the magnetosphere produces radiation in the X-ray band. The relaxation trend is determined by the evolution of the external twisted fields, and is demonstrated in Figure 10 of Beloborodov (2009) or in Figure 8 of Li et al. (2016). This may explain the early time trends in Figure 2. The time scale in the model is given by $t_\gamma = \mu/cR_*\bar{\mathcal{V}}$, where μ is the magnetic moment, c is the speed of light, R_* is the radius of the star, and $\bar{\mathcal{V}}$ is the average threshold voltage for discharge (see Beloborodov 2009, for more details). Assuming $B = 2 \times 10^{14}$ G, $R = 10$ km, and $\bar{\mathcal{V}} = 10^9$ V for SGR1627, t_γ is 10^9 s. Then the time for the flux to drop by an order of magnitude is $\approx 0.02t_\gamma \approx 200$ days similar to what we see in SGR1627. Further modeling would be needed to reproduce the shape of the flux decline in detail.

4. DISCUSSION AND CONCLUSIONS

We analyzed X-ray data from SGR1627 taken with *Chandra*, *XMM-Newton*, and *NuSTAR*. With these data, we constructed long-term cooling curves of the magnetar and studied the properties of the star and the outbursts using a crustal cooling model. We also studied the X-ray spectrum of SGR1627 and found evidence for a spectral turn-over at ~ 10 keV.

4.1. Hard X-ray Emission

In the data analysis including the *NuSTAR* data, we find evidence for hard X-ray excess in SGR1627. There are several possible causes of this if not the emission of the magnetar. CXOU J163547.0–473739 is too far off-axis to affect the results for the small source aperture we used for SGR1627 (Figure 1); only 0.25% (2 events in this case) contamination is expected into a $R = 20''$ circle at a distance of $2'$. The stray light and the ghost rays may be a larger concern (Figure 1; see Madsen et al. 2017, for more details). However, these backgrounds are soft, having a hardness ratio (count ratio in the 10–20 keV and the 3–10 keV bands) 0.12 ± 0.01 , while the ratio for SGR1627 is 0.63 ± 0.25 . With the positional coincidence between the hard excess and the soft-band detection, it is unlikely that the hard excess is produced by the stray light. Agreement between the *XMM-Newton* and the *NuSTAR* spectra in the common band further suggests that the detection may not be spurious. Moreover, in both cases, the background collected near the source position will have similar contamination and is subtracted in the spectral analysis. We therefore conclude that the spectral turn-over above 10 keV in SGR1627 may be real. However, the statistical significance for the turn-over is not very high, and further deep *NuSTAR* observations are needed to confirm the hard excess.

In some magnetars, a rising trend in the SED at $\gtrsim 10$ keV has been seen (Kuiper et al. 2006). Theoretically, the hard X-ray emission is explained with upscattering of soft thermal photons to higher energies $\gtrsim 10$ keV by outflow of $e^{+/-}$ plasma in the lower part of the magnetosphere (Beloborodov 2013). In this model, the hard X-ray spectral shape strongly depends on the viewing geometry, and the hard X-ray excess of SGR1627 suggests that its magnetic inclination may be modest (see Figure 7 of Beloborodov 2013); for inclinations less than 30° , 10–20 keV SEDs drop with energy. Further phase-resolved spectroscopy is required for the model to infer the inclination more precisely.

Observationally, Kaspi & Boydston (2010) found a correlation between magnetic field strength B and the degree of spectral break ($\Gamma_S - \Gamma_H$) in the magnetar population. Following their work, a break of ~ 2.5 is expected which is the same as we measure for the source if the hard excess is from the magnetar. Thus if the detection is real, SGR1627 can be added to the list of hard X-ray detected magnetars and possibly to the correlation found by Kaspi & Boydston (2010) for future population studies. It is interesting to note that the transient magnetar SGR1627 shows a possible hard X-ray turn-over in the quiescent state; perhaps other faint transient magnetars also show the turn-over in quiescence. If so, deep *NuSTAR* observations of these magnetars may be useful for population studies.

4.2. Flux Relaxation of SGR1627 Outbursts

With the new observations, we added flux measurements for SGR1627 after $\gtrsim 2000$ days into the outburst relaxation in order to study the late time relaxation trends of the magnetar using a crustal cooling model. These observations clearly show that the quiescent flux level is lower than is assumed by An et al. (2012), suggesting that the core temperature of SGR1627 may be low as originally proposed by Kouveliotou et al. (2003). We further show that the light curve of this magnetar exhibits another break at ~ 2000 days after the 2008 outburst, similar to what was seen in the same source after its 1998 outburst (Figure 2). We attempted to explain the flux relaxation with a crustal cooling model. While the model can explain the relaxation trends as in Deibel et al. (2017), it is hard to match the early trends in some other cases with crustal cooling only. This suggests that some other relaxation mechanisms such as magnetospheric untwisting (Beloborodov 2009) work simultaneously at early times (Section 3.2).

The locations of energy deposition in outbursts of magnetars can be different: the outside (Beloborodov & Li 2016), at shallow depth (Kaminker et al. 2006), or the inner crust (Li et al. 2016). In these models, energy is generated via mechanical failure in the crust (e.g., Perna & Pons 2011; Levin & Lyutikov 2012; Beloborodov & Levin 2014) and propagates inside, heating the star. Using simulations Beloborodov & Li (2016) and Li et al. (2016) suggested that heat deposition due to Hall-mediated avalanches and thermoplastic failures in magnetars should happen just below the outer parts of the crust at a depth $\gtrsim 100$ m from the surface (Beloborodov & Li 2016). The thermoplastic wave propagates fast and a long distance in their simulations, hence deposits heat deeper. If the whole stellar surface is heated by the outburst, our study of crustal cooling for the 2008 outburst of SGR1627 supports the scenario for the energy deposition in the inner crust as proposed by Beloborodov & Li (2016) and suggests that outburst energy may be deposited at different depths between outbursts. However, models with energy deposited in only a small fraction of the star or with the temperature limited to the melting temperature do not require the energy to be in the inner crust.

With the current data sets and models, it is hard to tell whether the whole surface, or only a small fraction is heated and thus another mechanism (e.g., magnetic untwisting) may operate at early times. These can be

further studied by measuring and modeling spectral evolution after outbursts. However, our crust model does not account for the spectral evolution yet because of complex interplay between the surface thermal emission and the magnetospheric plasma. In particular, the 1 keV effective temperature derived from our blackbody fits is much larger than the expected surface temperature in these models. Furthermore, the current data quality does not allow us to measure spectral evolution of the source during the relaxation. Further theoretical studies and high-quality observations are needed.

For the crustal cooling models, more outburst samples and further modeling works will help to break degeneracy in the models between the energy deposition profile and internal properties of neutron stars. Furthermore, measuring relaxation trends until very late times is an important probe for studying the deep interior of neutron stars which may contain interesting structure such as nuclear “pasta”. More detailed studies with a larger number of outbursts may give us new insights into the location of crustal failures, relaxation mechanisms, and the internal matter of neutron stars.

This research was supported by Basic Science Research Program through the National Research Foundation of Korea (NRF) funded by the Ministry of Science, ICT & Future Planning (NRF-2017R1C1B2004566). VMK is supported by an NSERC Discovery Grant and Herzberg Award, the Canadian Institute for Advanced Research, an FRQNT Centre Grant, a Canada Research Chair, and the Lorne Trottier Chair in Astrophysics & Cosmology. AC is supported by an NSERC Discovery Grant. AC thanks the School of Mathematics, Statistics, and Physics at Newcastle University for hospitality during completion of this work.

REFERENCES

- Akaike, H. 1974, *IEEE Transactions on Automatic Control*, 19, 716
- Alford, J. A. J., & Halpern, J. P. 2016, *ApJ*, 818, 122
- An, H., Kaspi, V. M., Tomsick, J. A., et al. 2012, *ApJ*, 757, 68
- An, H., Hascoët, R., Kaspi, V. M., et al. 2013, *ApJ*, 779, 163
- An, H., Archibald, R. F., Hascoët, R., et al. 2015, *ApJ*, 807, 93
- Anders, E., & Grevesse, N. 1989, *Geochim. Cosmochim. Acta*, 53, 197
- Balucinska-Church, M., & McCammon, D. 1992, *ApJ*, 400, 699
- Baring, M. G., & Harding, A. K. 2007, *Ap&SS*, 308, 109
- Beloborodov, A. M. 2009, *ApJ*, 703, 1044
- . 2013, *ApJ*, 762, 13
- Beloborodov, A. M., & Levin, Y. 2014, *ApJ*, 794, L24
- Beloborodov, A. M., & Li, X. 2016, *ApJ*, 833, 261
- Beloborodov, A. M., & Thompson, C. 2007, *ApJ*, 657, 967
- Bezchastnov, V. G., Haensel, P., Kaminker, A. D., & Yakovlev, D. G. 1997, *A&A*, 328, 409
- Cash, W. 1979, *ApJ*, 228, 939
- Corbel, S., Chapuis, C., Dame, T. M., & Durouchoux, P. 1999, *ApJ*, 526, L29
- de Jager, O. C., Raubenheimer, B. C., & Swanepoel, J. W. H. 1989, *A&A*, 221, 180
- Deibel, A., Cumming, A., Brown, E. F., & Reddy, S. 2017, *ApJ*, 839, 95
- Douchin, F., & Haensel, P. 2001, *A&A*, 380, 151
- Enoto, T., Shibata, S., Kitaguchi, T., et al. 2017, *ApJS*, 231, 8
- Esposito, P., Israel, G. L., Zane, S., et al. 2008, *MNRAS*, 390, L34
- Esposito, P., Burgay, M., Possenti, A., et al. 2009, *MNRAS*, 399, L44
- Fernández, R., & Thompson, C. 2007, *ApJ*, 660, 615
- Fornasini, F. M., Tomsick, J. A., Hong, J., et al. 2017, *ApJS*, 229, 33

- Gehrels, N. 1986, *ApJ*, 303, 336
- Gotthelf, E. V., & Halpern, J. P. 2007, *Ap&SS*, 308, 79
- Greenstein, G., & Hartke, G. J. 1983, *ApJ*, 271, 283
- Haensel, P., Kaminker, A. D., & Yakovlev, D. G. 1996, *A&A*, 314, 328
- Haensel, P., & Pichon, B. 1994, *A&A*, 283, 313
- Heyl, J. S., & Hernquist, L. 2005, *ApJ*, 618, 463
- Horowitz, C. J., Berry, D. K., Briggs, C. M., et al. 2015, *Physical Review Letters*, 114, 031102
- Itoh, N., & Kohyama, Y. 1993, *ApJ*, 404, 268
- Kaminker, A. D., Pethick, C. J., Potekhin, A. Y., Thorsson, V., & Yakovlev, D. G. 1999, *A&A*, 343, 1009
- Kaminker, A. D., Yakovlev, D. G., Potekhin, A. Y., et al. 2006, *MNRAS*, 371, 477
- Kaspi, V. M., & Beloborodov, A. M. 2017, *ARA&A*, 55, 261
- Kaspi, V. M., & Boydston, K. 2010, *ApJ*, 710, L115
- Kouveliotou, C., Eichler, D., Woods, P. M., et al. 2003, *ApJ*, 596, L79
- Kuiper, L., Hermsen, W., den Hartog, P. R., & Collmar, W. 2006, *ApJ*, 645, 556
- Levin, Y., & Lyutikov, M. 2012, *MNRAS*, 427, 1574
- Li, X., & Beloborodov, A. M. 2015, *ApJ*, 815, 25
- Li, X., Levin, Y., & Beloborodov, A. M. 2016, *ApJ*, 833, 189
- Loredo, T. J. 1992, in *Statistical Challenges in Modern Astronomy*, ed. E. D. Feigelson & G. J. Babu, 275–297
- Lyubarsky, Y., Eichler, D., & Thompson, C. 2002, *ApJ*, 580, L69
- Madsen, K. K., Christensen, F. E., Craig, W. W., et al. 2017, *Journal of Astronomical Telescopes, Instruments, and Systems*, 3, 044003
- Madsen, K. K., Harrison, F. A., Markwardt, C. B., et al. 2015, *ApJS*, 220, 8
- Mereghetti, S., Pons, J. A., & Melatos, A. 2015, *Space Sci. Rev.*, 191, 315
- Olausen, S. A., & Kaspi, V. M. 2014, *ApJS*, 212, 6
- Perna, R., & Pons, J. A. 2011, *ApJ*, 727, L51
- Pons, J. A., & Rea, N. 2012, *ApJ*, 750, L6
- Pons, J. A., Viganò, D., & Rea, N. 2013, *Nature Physics*, 9, 431
- Potekhin, A. Y., & Chabrier, G. 2000, *Phys. Rev. E*, 62, 8554
- Potekhin, A. Y., Pons, J. A., & Page, D. 2015, *Space Sci. Rev.*, 191, 239
- Potekhin, A. Y., & Yakovlev, D. G. 2001, *A&A*, 374, 213
- Rea, N., Esposito, P., Turolla, R., et al. 2010, *Science*, 330, 944
- Schinder, P. J., Schramm, D. N., Wiita, P. J., Margolis, S. H., & Tubbs, D. L. 1987, *ApJ*, 313, 531
- Scholz, P., Kaspi, V. M., & Cumming, A. 2014, *ApJ*, 786, 62
- Schwenk, A., Friman, B., & Brown, G. E. 2003, *Nuclear Physics A*, 713, 191
- Tendulkar, S. P., Hascöet, R., Yang, C., et al. 2015, *ApJ*, 808, 32
- Thompson, C., & Beloborodov, A. M. 2005, *ApJ*, 634, 565
- Thompson, C., & Duncan, R. C. 1995, *MNRAS*, 275, 255
- . 1996, *ApJ*, 473, 322
- Thompson, C., Lyutikov, M., & Kulkarni, S. R. 2002, *ApJ*, 574, 332
- Thompson, C., Yang, H., & Ortiz, N. 2017, *ApJ*, 841, 54
- Verner, D. A., Ferland, G. J., Korista, K. T., & Yakovlev, D. G. 1996, *ApJ*, 465, 487
- Vogel, J. K., Hascoët, R., Kaspi, V. M., et al. 2014, *ApJ*, 789, 75
- Wadiasingh, Z., Baring, M. G., Gonthier, P. L., & Harding, A. K. 2018, *ApJ*, 854, 98
- Wilms, J., Allen, A., & McCray, R. 2000, *ApJ*, 542, 914
- Woods, P. M., Kouveliotou, C., van Paradijs, J., et al. 1999, *ApJ*, 519, L139